J. Phys. B: At. Mol. Opt. Phys. **29** (1996) 779–790. Printed in the UK

Electron impact ionization of H_2^+

F Robicheaux
Department of Physics, Auburn University, Auburn, AL 36849, USA

Received 25 September 1995, in final form 9 November 1995

Abstract. The electron impact ionization cross section of H_2^+ is calculated using a distorted-wave approximation. The calculated cross section is compared to the experimental results of Peart and Dolder. The simplicity of the system allows an assessment of the accuracy of the distorted-wave approximation without complications from inaccuracies in the target state, initial continuum state, or final continuum states. The agreement with experiment is poor at low energies but improves substantially at higher energies. A differential cross section at an incident electron energy of 103 eV is presented. The proton energy distribution after the ionization is presented for large incident electron energy.

1. Introduction

Calculations that are relatively simple for atomic neutral or ionic species can be much more difficult for molecular neutral or ionic species. It is useful to assess the accuracy of crude theoretical methods to provide a gauge of the quality of calculations. For this purpose, first-order distorted wave calculations for electron impact ionization of H_2^+ are presented. This molecular system was chosen for the simplicity of the electronic structure and the availability of experimental results. The errors in the calculation must arise from the deficiencies of the first-order, distorted-wave method. For more complicated systems, it could be argued that errors are due to inaccuracies in the distorted waves, in the target states, or in the scattered waves.

The fixed-nuclei electronic states of H_2^+ can be calculated to arbitrary accuracy using prolate spheroidal coordinates. The simplicity of the states and the interaction potential allows the calculation to proceed with modest investment in computational resources. Therefore, it is somewhat surprising that these are the first fully quantum calculations of this process although experimental results have been available for over 20 years.

Peart and Dolder (1973) measured the electron impact ionization cross section of H_2^+ by detecting the simultaneous arrival of two protons in a scintillation detector. Two protons are always liberated when H_2^+ is ionized in the reaction:

$$H_2^+(1s\sigma_g) + e^- \rightarrow 2p + 2e^-. \qquad \text{(a)}$$

By detecting the simultaneous arrival of *two* protons, they were able to distinguish the process (a) from protons liberated by the reaction

$$H_2^+(1s\sigma_g) + e^- \rightarrow H(n\ell) + p + e^-. \qquad \text{(b)}$$

The number of protons produced in the second reaction vastly outnumber those produced in the first reaction. The protons from the different reactions, (a) and (b), were distinguished by

0953-4075/96/040779+12$19.50

the pulse height they created in the detector. Pulse heights from the first reaction were twice as large as those from the second because two protons arrive simultaneously in reaction (a).

The present calculations were performed in prolate spheroidal coordinates with the protons fixed in space at an internuclear distance $R = 2.15$ au which is 0.15 au larger than the equilibrium separation of H_2^+ in the ground vibrational state. This distance was chosen in order to match $\langle R \rangle$ using the experimental vibrational distribution. A discussion of the accuracy of this procedure is presented below. The methods used to produce the electronic wavefunctions numerically and carry out the Slater integrals in prolate spheroidal coordinates are also discussed. The formula for the ionization cross section in prolate spheroidal coordinates is presented with reference to energy normalized continuum functions. The asymptotic form of energy normalized prolate spheroidal continuum functions is also given. Various tests of the computer programs are described.

2. Single-electron wavefunctions

2.1. Coordinate system and Hamiltonian

The wavefunction for an electron in the field of two stationary point charges can be simply obtained in prolate spheroidal coordinates (Judd 1975). (The vast literature pertaining to H_2^+ and its electronic states in prolate spheroidal coordinates cannot be adequately referenced. For early large-scale computations see Bates *et al* (1953) and Bates and Reid (1968).) If one charge is at the position $\boldsymbol{R}_1 = (0, 0, R/2)$ and the other at $\boldsymbol{R}_2 = (0, 0, -R/2)$, where R is the distance between the charges, then the prolate spheroidal coordinates are given by

$$\begin{aligned} \xi &= (|\boldsymbol{r} - \boldsymbol{R}_2| + |\boldsymbol{r} - \boldsymbol{R}_1|)/R \\ \eta &= (|\boldsymbol{r} - \boldsymbol{R}_2| - |\boldsymbol{r} - \boldsymbol{R}_1|)/R \\ \varphi &= \arctan(y/x) \end{aligned} \tag{1}$$

where $\boldsymbol{r}$ is the position vector of the electron measured from the origin. The coordinate ξ is the analogue of the radial coordinate and η is the analogue of $\cos\theta$; for large r, $\xi = 2r/R$ and $\eta = \cos\theta$. The volume element used for the integrations is

$$\mathrm{d}V = \mathrm{d}x\,\mathrm{d}y\,\mathrm{d}z = \left(\frac{R}{2}\right)^3 (\xi^2 - \eta^2)\mathrm{d}\xi\,\mathrm{d}\eta\,\mathrm{d}\varphi \tag{2}$$

where ξ ranges from 1 to ∞; η ranges from -1 to 1; φ ranges from 0 to 2π.

For an electron moving in the field of two stationary protons at $\boldsymbol{R}_1$ and $\boldsymbol{R}_2$, the Hamiltonian is (in atomic units)

$$\begin{aligned} H_0 &= -\tfrac{1}{2}\nabla^2 - 1/|\boldsymbol{r} - \boldsymbol{R}_1| - 1/|\boldsymbol{r} - \boldsymbol{R}_2| \\ &= -\frac{2}{R^2}\frac{1}{\xi^2 - \eta^2}\left[\frac{\partial}{\partial\xi}(\xi^2 - 1)\frac{\partial}{\partial\xi} + \frac{\partial}{\partial\eta}(1 - \eta^2)\frac{\partial}{\partial\eta} + \frac{\xi^2 - \eta^2}{(\xi^2 - 1)(1 - \eta^2)}\frac{\partial^2}{\partial\varphi^2}\right] \\ &\quad -\frac{4\xi}{R}\frac{1}{\xi^2 - \eta^2}\,. \end{aligned} \tag{3}$$

The two-electron wavefunctions in the present calculation will be approximated by products of one-electron wavefunctions with the appropriate symmetry. One-particle wavefunctions that are solutions of

$$H_0\psi(\boldsymbol{r}) = E\psi(\boldsymbol{r}) \tag{4}$$

can be obtained in the form

$$\psi_{E\lambda m} = F_{E\lambda m}(\xi)\mathcal{Y}_{E\lambda m}(\eta, \varphi) \tag{5}$$

where

$$\frac{1}{\mathrm{i}}\frac{\partial}{\partial\varphi}\mathcal{Y}_{E\lambda m}(\eta, \varphi) = m\mathcal{Y}_{E\lambda m}(\eta, \varphi) \tag{6a}$$

$$\left[\frac{\partial}{\partial\eta}(1-\eta^2)\frac{\partial}{\partial\eta} + f_{E\lambda m} - \frac{ER^2}{2}\eta^2 - \frac{m^2}{1-\eta^2}\right]\mathcal{Y}_{E\lambda m}(\eta, \varphi) = 0 \tag{6b}$$

$$\left[\frac{\partial}{\partial\xi}(\xi^2-1)\frac{\partial}{\partial\xi} - f_{E\lambda m} + \frac{ER^2}{2}\xi^2 + 2R\xi - \frac{m^2}{\xi^2-1}\right]F_{E\lambda m}(\xi) = 0\,. \tag{6c}$$

This is the main advantage of using prolate spheroidal coordinates; the wavefunction for one electron in the field of two stationary protons separates in these coordinates.

The $\mathcal{Y}_{E\lambda m}(\eta, \varphi)$ functions are the analogue of the spherical harmonics and are normalized such that

$$\int_{-1}^{1}\mathrm{d}\eta\int_{0}^{2\pi}\mathrm{d}\varphi\,\mathcal{Y}^{*}_{E\lambda m}(\eta, \varphi)\mathcal{Y}_{E\lambda' m'}(\eta, \varphi) = \delta_{mm'}\delta_{\lambda\lambda'}\,. \tag{7}$$

These functions are obtained by expanding in a basis of spherical harmonics

$$\mathcal{Y}_{E\lambda m}(\eta, \varphi) = \sum_{\ell} Y_{\ell m}(\eta, \varphi)U^{m}_{\ell\lambda}(E) \tag{8}$$

with the coefficients of the basis function obtained by numerically diagonalizing a real symmetric matrix. For the calculations reported here it was not necessary to go higher than the $\ell = 19$ harmonic to obtain convergence in the ionization cross section. The off-diagonal matrix elements only couple ℓ to $\ell \pm 2$ so the even ℓ and odd ℓ states can be obtained separately. As $ER^2 \to 0$ the $\mathcal{Y}_{E\lambda m}$ become equivalent to spherical harmonics; part of the difficulty calculating high energy wavefunctions arose from the strong departure of the $\mathcal{Y}_{E\lambda m}$ from spherical harmonics due to the large coupling from the $ER^2\eta^2/2$ term in (6*b*); this complicated the calculation of the $1/r_{12}$ matrix elements. However, the diagonalization never involved a matrix larger than 10×10 which made the calculation of the angular functions rather trivial.

It was more difficult to obtain the $F_{E\lambda m}(\xi)$ functions then the $\mathcal{Y}$ functions; however, these functions, F, are solutions of a linear second-order differential equation so they could be obtained fairly easily. The difficulty with the F functions is that they depend on λ *and* $|m|$ which increases the number that need to be calculated (over the number of radial functions that would be needed in spherical coordinates). The first derivative terms in (6*c*) can be eliminated by solving for the function $G_{E\lambda m}(\xi)$ defined by

$$F_{E\lambda m}(\xi) = G_{E\lambda m}(\xi)/\sqrt{\xi^2-1}\,. \tag{9}$$

This is analogous to solving for $R(r) = u(r)/r$ in spherical coordinates. The differential equation for $G_{E\lambda m}(\xi)$ is

$$\left[\frac{\partial^2}{\partial\xi^2} + k^2_{E\lambda m}(\xi)\right]G_{E\lambda m}(\xi) = 0 \tag{10}$$

where

$$k^2_{E\lambda m}(\xi) = \left(-f_{E\lambda m} + \frac{ER^2}{2}\xi^2 + 2R\xi - \frac{m^2-1}{\xi^2-1} \right) / (\xi^2 - 1) \,. \tag{11}$$

The differential equation for G gives a function which has a square root singularity at $\xi = 1$ and an essential singularity at $\xi \to \infty$ when $E \neq 0$. At very large distances, $\xi \to \infty$

$$k^2_{E\lambda m}(\xi) \to \frac{ER^2}{2} + \frac{2R}{\xi} - \frac{f_{E\lambda m} - ER^2/2}{\xi^2} \tag{12}$$

which has the form of a Coulomb potential but with non-integer angular momentum. Note the combination $ER^2/2 = (kR/2)^2$ where k is the wavenumber of the electron. The numerical procedure for obtaining the solutions of (10) is described in the appendix.

2.2. Normalization of single electron functions

In the formula for T-matrix elements described in the next section, the ground-state target function is normalized per unit volume and the continuum waves are normalized per unit energy. The ground state wavefunction has the form

$$\psi_{E_g\lambda_g m_g}(\xi, \eta, \varphi) = N F_{E_g\lambda_g m_g}(\xi) \mathcal{Y}_{E_g\lambda_g m_g}(\eta, \varphi) \tag{13}$$

which means

$$\int \mathrm{d}V |\psi_{E_g\lambda_g m_g}|^2 = \frac{N^2R^3}{8} \int_1^\infty \mathrm{d}\xi \int_{-1}^1 \mathrm{d}\eta \int_0^{2\pi} \mathrm{d}\varphi (\xi^2 - \eta^2) F^2_{E_g\lambda_g m_g}(\xi) |\mathcal{Y}_{E_g\lambda_g m_g}(\eta, \varphi)|^2 = 1 \,. \tag{14}$$

The angular part of this integration was obtained from the coefficients of the expansion of $\mathcal{Y}$ in spherical harmonics and analytic matrix elements involving the $Y_{\ell m}$.

A non-rigorous derivation of the form of the continuum wavefunction for energy normalization can be obtained by a simple comparison to energy normalized functions in radial coordinates. In radial coordinates the asymptotic form of the wavefunction is

$$\sqrt{\frac{2}{\pi k r^2}} Y_{\ell m}(\cos\theta, \varphi) \sin(kr + \delta_{E\ell}(r)) \tag{15}$$

where $E = k^2/2$. The correspondence between spherical and spheroidal coordinates ($r \to \xi R/2$, $\cos\theta \to \eta$) gives an asymptotic form

$$\sqrt{\frac{8}{\pi k R^2 \xi^2}} \mathcal{Y}_{E\lambda m}(\eta, \varphi) \sin\left(\frac{kR}{2}\xi + \delta_{E\lambda m}(\xi) \right) . \tag{16}$$

A more rigorous (and much lengthier) derivation using Green's theorem in the spirit of Fano and Rau (chapter 5.7) gives exactly the same form. The normalization of the numerical functions could be obtained by matching them to Coulomb functions from standard computer programs because the asymptotic form of the differential equation for G is the same as for Coulomb functions with non-integer ℓ. However, the overall speed of the program and the number of continuum waves that needed to be calculated forced the use of an approximation. The normalization of the $G_{E\lambda m}(\xi)$ was obtained by matching to a WKB solution of (10) with the asymptotic form

$$G_{E\lambda m}(\xi) \sim \left[\frac{4}{\pi R k_{E\lambda m}(\xi)} \right]^{1/2} \sin\left(\int^\xi k_{E\lambda m}(\xi') \mathrm{d}\xi' + \delta_{E\lambda m} \right) . \tag{17}$$

This is a good approximation for the calculations reported here because the energies of the continuum waves are relatively large compared to the potential energies at the matching distance.

3. *T*-matrix elements and cross section

3.1. Fixed-nuclei approximation

A frozen-nuclei approximation was used to calculate the cross section. This is a good approximation because the electrons' speeds are at least 30 times greater than that of the nuclei. The cross section can be approximated by $\langle\sigma_{\rm I}(E;R)\rangle$ where $\sigma_{\rm I}(E;R)$ is the ionization cross section calculated with fixed nuclei separated by a distance R and $\langle\,\rangle$ indicates averaging over the initial R distribution. The ionization cross section increases with the internuclear distance in a roughly linear fashion near $R = 2$ au. At small R, H_2^+ looks like He^+ which has a smaller ionization cross section than for H (large R). Because the cross section has a roughly linear dependence on R, it is only necessary to calculate the cross section at the distance $R_{\rm ave} = \langle R\rangle = 2.15$ au which is 0.15 au greater than the distance of the potential minimum. The average distance was obtained from the vibrational distribution of von Busch and Dunn (1972); Peart and Dolder state the vibrational distribution in their experiment should be similar to theirs. The approximation that is being made is $\langle\sigma_{\rm I}(E;R)\rangle = \sigma_{\rm I}(E;R_{\rm ave}) + {\rm O}[\langle(R-R_{\rm ave})^2\rangle]$. Numerical tests for the low-energy cross section (which is most sensitive to R) found the approximation worked to better than 1%. The implications of this approximation for the energy distribution of the protons are discussed in the results section.

3.2. Fixed-nuclei matrix elements

When using energy normalized wavefunctions, the distorted wave T-matrix element connecting channels i and j is

$$T_{ij} = \pi\langle\psi_i|E - H|\psi_j\rangle \tag{18}$$

where the ket $\langle\psi_i|$ does not mean complex conjugation of the radial functions. The continuum parts of the ψ_i and ψ_j functions have T-matrix form in the asymptotic region. The ionization cross section can be obtained simply by analogy to excitation if all of the continuum waves are energy normalized.

Let E_i be the energy of the incident electron, E_g be the energy of the target electron in the ground state, and E_1 and E_2 be the energies of the two continuum electrons after the collision. Conservation of energy gives $E_i + E_g = E_1 + E_2 = E_{\rm T}$ where $E_{\rm T}$ is the total electronic energy. All of the energies in this equation are electronic energies only. This equation supposes the electrons do not exchange energy with the protons during the ionization process. Within this approximation the protons will have a centre of mass energy distribution peaked near 6 eV in a way that depends on the initial vibrational distribution of H_2^+. (An approximate proton energy distribution is given in the results section.) The total ionization cross section (in atomic units) can be written as

$$\sigma_{\rm I}(E_i) = \frac{1}{2}\int_0^{E_{\rm T}} \frac{{\rm d}\sigma_{\rm I}}{{\rm d}E_2}\,{\rm d}E_2 \tag{19}$$

where

$$\frac{{\rm d}\sigma_{\rm I}}{{\rm d}E_2} = \frac{2\pi^3}{E_i}\sum_{\lambda_i m_i \lambda_1 m_1 \lambda_2 m_2}\{|I(i,g;1,2)|^2 + |I(g,i;1,2)|^2 - I^*(i,g;1,2l)I(g,i;1,2)\} \tag{20}$$

with $E_1 = E_T - E_2$ and

$$I(i, g; 1, 2) = -\int dV_1 \int dV_2 \psi^*_{E_i\lambda_i m_i}(\boldsymbol{r}_1)\psi^*_{E_g\lambda_g m_g}(\boldsymbol{r}_2)\frac{1}{r_{12}}\psi_{E_1\lambda_1 m_1}(\boldsymbol{r}_1)\psi_{E_2\lambda_2 m_2}(\boldsymbol{r}_2)\,. \tag{21}$$

The complex conjugation in (21) does not apply to the F functions. The simple form of (20) results from two drastic approximations: (i) the ground-state wavefunction and the wavefunctions for the scattered and ejected wave are obtained from the same local Hamiltonian (equation (5)) which means they are orthogonal to each other (no one-body interaction terms survive). (ii) *all* of the continuum waves are solved within a local potential which does not depend on the total spin; therefore, the continuum waves for singlet and triplet spin couplings are identical.

The energy integration in (19) is accomplished through a seven-point Gaussian quadrature. Convergence was tested by comparing to a five-point Gaussian quadrature. (The differential cross section in (20) is symmetric about $E_2 = E_T/2$ and therefore $d\sigma_I/dE_2$ was only calculated at four points in E_2 for every energy of the incoming electron E_i.) The sums in (20) were kept to as small a range as possible consistent with three-digit accuracy in the calculated cross section. For the lowest incident energies all of the $\lambda, m \leqslant 10$. For the highest energies all of the $\lambda, m \leqslant 19$.

4. Slater integrals

The integrations in (21) are carried out in spheroidal coordinates to take advantage of the simplicity of the orbitals in this coordinate system. Fortunately, the $1/r_{12}$ operator has a partial-wave-type expansion in spheroidal coordinates. This expansion is

$$\frac{1}{r_{12}} = \frac{8\pi}{R}\sum_{\ell m}(-1)^m Q^m_\ell(\xi_>)P^m_\ell(\xi_<)Y_{\ell,m}(\eta_1, \varphi_1)Y_{\ell,-m}(\eta_2, \varphi_2) \tag{22}$$

where the $Q^m_\ell(\xi)$ ($P^m_\ell(\xi)$) are the irregular (regular) Legendre functions with asymptotic form (as $\xi \to \infty$)

$$Q^m_\ell(\xi) \to \xi^{-\ell-1}2^\ell \ell!(\ell+m)!/(2\ell+1)! \tag{23}$$

$$P^m_\ell(\xi) \to \xi^\ell(2\ell)!/[2^\ell \ell!(\ell-m)!]\,. \tag{24}$$

The integral that enters the cross section $I(\cdots)$ has the form

$$\mathrm{I}(i, g; 1, 2) = \left(\frac{R}{2}\right)^6 \frac{8\pi}{R}\sum_{\ell m}\int_1^\infty d\xi_1 \int_1^\infty d\xi_2 Q^m_\ell(\xi_>)P^m_\ell(\xi_<)F_1(\xi_1)F_2(\xi_2) \tag{25}$$

where

$$F_1(\xi) = F_{E_i\lambda_i m_i}(\xi)F_{E_1\lambda_1 m_1}(\xi)(\xi^2 B^{\ell m}_{E_i\lambda_i m_i, E_1\lambda_1 m_1} - C^{\ell m}_{E_i\lambda_i m_i, E_1\lambda_1 m_1}) \tag{26}$$

with

$$B^{\ell m}_{E_i\lambda_i m_i, E_1\lambda_1 m_1} = (-1)^{\mu+m}\sum_{\ell_i\ell_1} U^{m_i}_{\ell_i\lambda_i}U^{m_1}_{\ell_1\lambda_1}\sqrt{\frac{(2\ell_i+1)(2\ell+1)(2\ell_1+1)}{4\pi}}$$
$$\times \begin{pmatrix} \ell_i & \ell & \ell_1 \\ 0 & 0 & 0 \end{pmatrix}\begin{pmatrix} \ell_i & \ell & \ell_1 \\ -m_i & m & m_1 \end{pmatrix} \tag{27}$$

$$C^{\ell m}_{E_i\lambda_i m_i, E_1\lambda_1 m_1} = \frac{2}{R^2 E_1}(-1)^{\mu+m}\sum_{\ell_i\ell_1} U^{m_i}_{\ell_i\lambda_i} U^{m_1}_{\ell_1\lambda_1}\sqrt{\frac{(2\ell_i+1)(2\ell+1)(2\ell_1+1)}{4\pi}}$$
$$\times [f_{E_1\lambda_1 m_1} - \ell_1(\ell_1+1)]\begin{pmatrix}\ell_i & \ell & \ell_1\\ 0 & 0 & 0\end{pmatrix}\begin{pmatrix}\ell_i & \ell & \ell_1\\ -m_i & m & m_1\end{pmatrix} \tag{28}$$

where F_2 has a structure similar to F_1 with the replacement $i \to g$ and $1 \to 2$.

The standard method for calculating integrals of the form (25) is to rewrite the integrals as

$$\int_1^\infty \mathrm{d}\xi_1\, F_1(\xi_1) v_{\ell m}(\xi_1) \tag{29}$$

where the function $v_{\ell m}$ is the analogue in spheroidal coordinates of the Hartree y-function. The usual method for obtaining this function for atoms is to write $v_{\ell m}(\xi)$ as the solution of a first-order differential equation. This method is not used here because it is more time consuming to calculate the P and Q Legendre functions than r^ℓ and $1/r^{\ell+1}$ which appear in atomic Slater integrals. The $v_{\ell m}$ were instead obtained as solutions of a second-order inhomogeneous equation given by

$$\left[\frac{\mathrm{d}}{\mathrm{d}\xi}(\xi^2-1)\frac{\mathrm{d}}{\mathrm{d}\xi} - \ell(\ell+1) - \frac{m^2}{\xi^2-1}\right] v_{\ell m}(\xi) = -F_2(\xi) \tag{30}$$

with the condition that as $\xi \to \infty$

$$v_{\ell m}(\xi) \to \bar{v}_{\ell m}/\xi^{\ell+1}\,. \tag{31}$$

Because equation (30) has the same form as (6*c*) but with an inhomogeneous term, it was relatively trivial to modify the subroutines that calculated the solution of (6*c*) so that the $v_{\ell m}$ could be obtained.

It was important to calculate the $v_{\ell m}$ and integrate (29) as quickly as possible because of the number of times these operations need to be carried out at each energy. Because of the dependence on the magnetic quantum number in all of the functions of ξ, all operations need to be carried out many orders of magnitude more often than in a similar calculation for a one-electron atom. One of the methods used to speed the calculation was to order the wavefunctions in a way that reduced to one the number of times the $v_{\ell m}$ needed to be calculated. The ordering and speed of the operations were such that the calculation of the $F_1(\xi)$ function was the slow step of the procedure.

One of the tests of the code was that $\bar{v}_{00} = 0$ for all of the integrals needed for the ionization cross section. In general, the calculated $\bar{v}_{00} < 10^{-5}$. Another problem, is that unlike atomic calculations there are no sharp selection rules connecting ℓ, λ_i, and λ_1. In the calculation, the sum in (25) was truncated at $\ell, m \leqslant 4$. The higher ℓ did not contribute to the cross section at the 0.1% level.

The summation in (20) involves several different variables. Symmetry requirements force many of the terms to be identical; the simplest of these symmetries is the simultaneous reversal of the sign of all of the magnetic quantum numbers. Computational speed forced the code to be written to take advantage of these symmetries. In order to check all aspects of the code, the internuclear distance was reduced to $R = 10^{-3}$ au. The ionization cross section from this program was compared to that from an atomic distorted-wave program for He^+. The differential and total cross sections from the program in prolate spheroidal

coordinates matched those for the atomic physics program to better than 0.1%. This gives confidence that no gross errors have been made in the molecular ionization program.

5. Results

In figure 1, the electron impact ionization cross section is presented as a function of energy. The experimental points are from Peart and Dolder (1973). The error bars are the statistical errors that were quoted. Peart and Dolder assessed their systematic errors to be less than 6% which means the experiments and calculations are in perfect agreement for incident energies $\geqslant$ 88 eV. The diamonds are for distorted-wave calculations where *all* of the continuum waves (including the incident wave) are calculated in the field of two stationary protons. The squares are for distorted-wave calculations where a local screening potential was used for the incident wave but the ejected and scattered waves were calculated in the field of two protons. The results for the screened incident wave were not very sensitive to the form of the screening potential; basically, the same cross section was obtained (within 2%) if the incident wave was calculated for a field generated by two charge $\frac{1}{2}$ particles or by a true screening potential. The difference between the two calculations in figure 1 gives an estimate of the error in the distorted-wave method.

The major differences between the two distorted-wave calculations and the experiment are at low energy which is not very surprising. At lower energies the electrons interact more strongly which reduces the accuracy of a first-order perturbative method. It is encouraging that the distorted-wave calculations and the experiment are in excellent agreement for energies $\geqslant$ 88 eV. This shows that an 'exact' implementation of distorted-wave methods can reproduce the physics at relatively low energy (less than three times the threshold energy).

Both of the calculated cross sections are too large at lower energies. This suggests a second-order process is becoming more important for these energies. Two possible mechanisms could reduce the ionization cross section: (i) de-excitation of a continuum

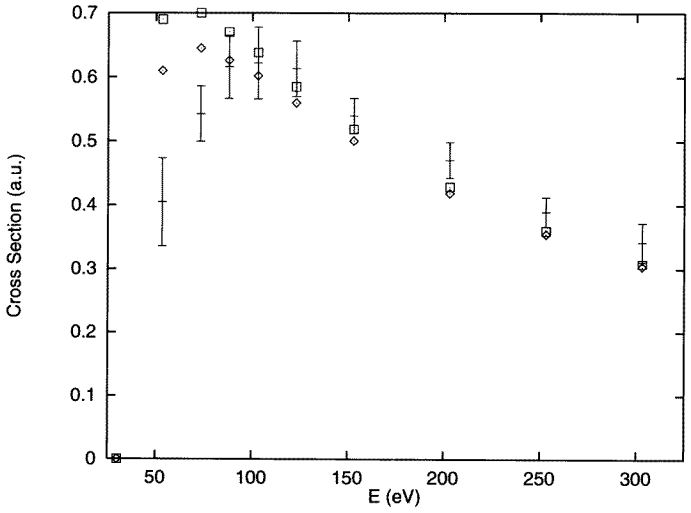

Figure 1. The total ionization cross section of H_2^+ as a function of incident electron energy. The experimental points are from Peart and Dolder (1973). The diamonds are distorted-wave results when all of the continuum waves are calculated in the field of two stationary protons. The squares are distorted wave results when the incident wave moves in a screened potential.

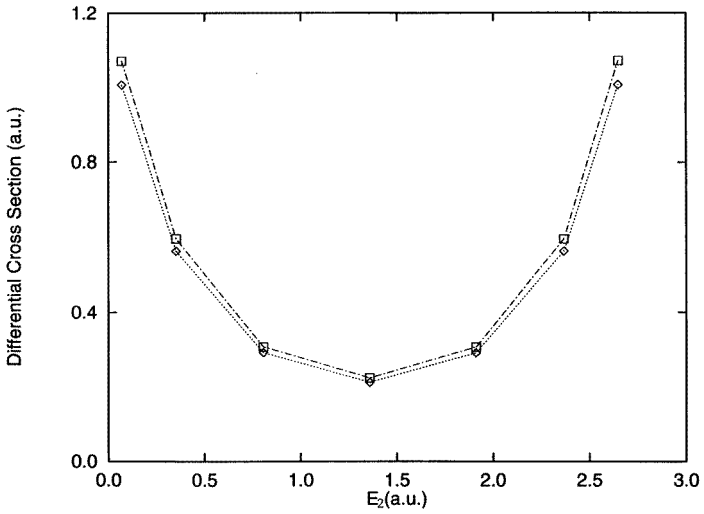

Figure 2. The differential cross section, $d\sigma_1/dE_2$, at an incident energy of 103 eV. The symbols are the same as in figure 1.

electron into a bound state, (ii) excitation of ground-state electron into excited states which removes ground-state probability thus reducing the ionization cross section. Unfortunately, second-order ionization processes are too difficult to implement for molecules so the reason for the failure of the distorted-wave method is unknown. It seems more likely that de-excitation of a continuum electron into bound states causes the reduction in the ionization cross section.

The calculation presented in figure 1 illustrates the good agreement between the experiments and distorted waves for the total cross section. However, total cross sections are notoriously insensitive to approximations in the calculation. In figure 2, the differential cross section $d\sigma_1/dE_2$ is presented at an incident energy of 103 eV. The symbols are the same as those in figure 1. Unfortunately, at this time there are no experimental results to compare with the calculation. The shape of the differential cross section is fairly typical of direct ionization processes at several times threshold energy. The cross section is much larger for the energies where one of the electrons moves slowly and smaller for both electrons sharing the energy equally. This cross section would be a more sensitive test of the distorted-wave calculation. The cross section is symmetric about the average electron energy $(E_1 + E_2)/2$ as it must be.

Another test of the assumptions in this paper derives from a measurement of the distribution of proton energies after the ionization process. The calculations presented here assume that the ionization process occurs extremely fast compared to the nuclear motions. Within this picture, the nuclei are initially bound together by one of the electrons. During the ionization, they are 'instantly' stripped of this electron after which they move on a repulsive $1/R$ potential. The distribution of final energies will be given by a projection of the nuclear wavefunction before the ionization onto the nuclear wavefunction after the ionization:

$$P(E) = \sum_v P_v \left[\int_0^\infty F_{2E}(R)\chi_v(R)\,dR \right]^2 \tag{32}$$

where P_v is the probability for the H_2^+ ion to initially be in the v vibrational state (taken

from table 2, column (C) of von Busch and Dunn), $\chi_v(R)$ is the vth vibrational function for H_2^+, and $F_{2E}(R)$ is the continuum wavefunction for two protons at centre of mass energy $2E$ (each proton carries half of the energy).

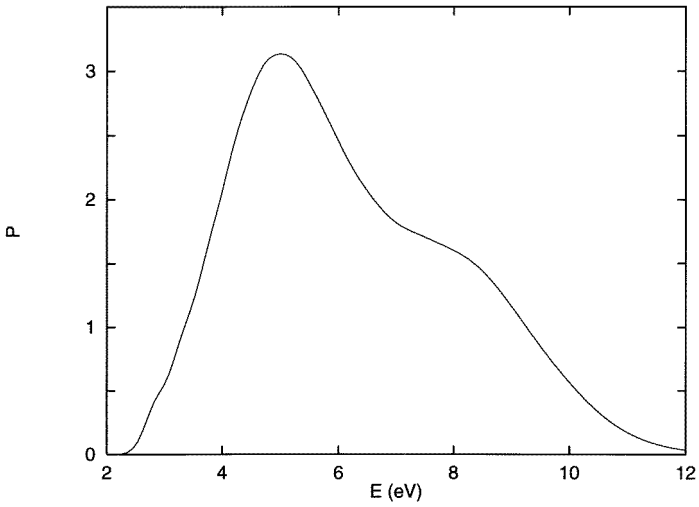

Figure 3. Approximate distribution of proton energies in the frame where the centre of mass is stationary. This distribution will become increasingly inaccurate as the incident electron energy is lowered.

The approximate proton energy distribution is given in figure 3. This distribution is surprisingly broad which reflects the slow reduction of P_v with increasing v. The peak of this distribution mainly arises from the fact that the two protons are initially at $R \sim 2.15$ au with roughly zero kinetic energy giving an energy of 0.5×27.2 eV$/2.15 = 6.3$ eV. The distribution of proton energies from (32) does not depend on the incident electron energy. This approximation will begin to substantially fail when the width of the proton distribution becomes comparable to $(E_1 + E_2)/2$ (the average of the ejected and scattered electron energies). The width of the proton distribution is ~ 5 eV. The average electron energy is given to a good approximation by $(E_i - 30$ eV$)/2$. An examination of figure 1 indicates the stationary nuclei approximation may be failing at the lower two energy points.

6. Conclusions

The present calculations do not uncover any surprises. However, the comparison gives a clear estimate of the accuracy of the distorted-wave method when it can be applied exactly. The calculated cross section is substantially larger than the experimental cross section at the two low energy points: 53.4 and 73.4 eV energy for the incident electron. At higher energies ($>$110 eV) the calculated cross section is uniformly $\sim 7\%$ smaller than the experimental cross section. The systematic errors of the experiment were assessed to be less than 6% and the random errors were between 5% and 15%. The calculated and experimental cross section are in perfect agreement for incident electron energies $\geqslant 88$ eV. The maximum value of the ionization cross section is exactly reproduced.

The exact implementation of the distorted-wave calculation of electron impact ionization reproduces the experimental cross section for incident energies three times greater than the threshold energy for ionization. The discrepancies at smaller energies are an intrinsic feature of the distorted-wave method and cannot be attributed to inaccuracies in the target state wavefunction, etc. A cross section differential in energy has been presented which may further probe the accuracy of the method since it is at an energy where the agreement is apparently perfect for the total ionization cross section. The distribution of proton energies has been presented for the same reason. The results of this paper indicate that an accurate implementation of the distorted-wave method can give very accurate results for molecules at relatively low energy.

Acknowledgments

I thank M Pindzola for several useful discussions and for providing distorted-wave electron impact ionization cross sections for He^+. I would like to acknowledge discussions with J Macek about some limitations of perturbation theory with Coulomb field perturbations and discussions with C H Greene about the difficulties in solving (6*c*). This work was supported by the US Department of Energy under grant number DE-FC02-91ER75678.

Appendix

The numerical solution of (10) must be handled carefully because of the singularity at $\xi = 1$. Part of the difficulty can be avoided by using a square root mesh. Instead of solving for $G_{E\lambda m}(\xi)$ as a function of ξ, the solution is obtained as a function of s where

$$\xi = 1 + s^2 \qquad \text{and} \qquad \mathrm{d}\xi = 2s\,\mathrm{d}s \tag{A1}$$

with $s \geqslant 0$. The differential equation that needs to be solved is

$$\left[\frac{\mathrm{d}^2}{\mathrm{d}s^2} - \frac{1}{s}\frac{\mathrm{d}}{\mathrm{d}s} + 4s^2 k_{E\lambda m}^2 (1 + s^2)\right] G_{E\lambda m}(s) = 0 \tag{A2}$$

where the points are equally spaced in s, i.e. the jth point is $s_j = j\Delta s$. This is a good compromise mesh for continuum waves because there are more points near the singularity than for a linear mesh but the largest step in ξ is only twice as big as for a linear mesh. A Numerov-type algorithm accurately propagates (A2). In general, the solution of a differential equation of the form

$$y''(x) - \frac{1}{x}y'(x) = A(x)y(x) + S(x) \tag{A3}$$

can be propagated with a Numerov-type procedure

$$y(x+\Delta) = \left\{y(x)\left[2 + \Delta^2 A(x)\left(\frac{5}{6} - \frac{\Delta^2}{4x^2}\right)\right] - y(x-\Delta)\left(1 + \frac{\Delta}{2x}\right)\left[1 - \frac{\Delta^2}{12}A(x-\Delta)\right] + \Delta^2 Q(x)\right\} \Big/ \left\{\left(1 - \frac{\Delta}{2x}\right)\left[1 - \frac{\Delta^2}{12}A(x+\Delta)\right]\right\} + \mathrm{O}(\Delta^5) \tag{A4}$$

where

$$Q(x) = \frac{1}{12}\left(1 - \frac{\Delta}{2x}\right)S(x+\Delta) + \frac{1}{12}\left(1 + \frac{\Delta}{2x}\right)S(x-\Delta) + \left(\frac{5}{6} - \frac{\Delta^2}{4x^2}\right)S(x)\,. \tag{A5}$$

Equation (A4) has errors of $O(\Delta^5)$ (instead of $O(\Delta^6)$ for the ordinary Numerov propagator) because $1/x$ is order $1/\Delta$ near $x = 0$.

The propagator given in (A4) produces accurate functions except for $m = 0$. The source of the difficulty derives from the behaviour of $G_{E\lambda m}(s)$ near $s = 0$. The regular solution goes like $s^{|m|+1}$ while the irregular solution goes like $s^{-|m|+1}$. For $m = 0$ the regular and irregular solutions go like s and $s \log s$. Starting the propagation with $G_{E\lambda m}(0) = 0$ and $G_{E\lambda m}(\Delta) = \Delta^{|m|+1}$ will not work for $m = 0$ since the irregular solution can have these first two points as well (irregular solution $s \log s / \log \Delta$). This difficulty was surmounted by utilizing a ten-term power-series expansion for $G_{E\lambda m}$ when $m = 0$. The power series was used for distances small enough that errors from the truncation were less than a part in 10^6. Equation (A4) was used to propagate the $m = 0$ solution to larger distances.

The accuracy of the propagation scheme was tested by calculating the bound state energies of H_2^+ for $m = 0$ and $m = 1$. Five digit accuracy could be obtained with less than 400 mesh points.

References

Bates D R, Ledsham K and Stewart A L 1953 *Phil. Trans. R. Soc.* A **246** 215
Bates D R and Reid R H G 1968 *Adv. At. Mol. Phys.* **4** 13
Fano U and Rau A R P 1986 *Atomic Collisions and Spectra* (Orlando, FL: Academic)
Judd B R 1975 *Angular Momentum Theory for Diatomic Molecules* (New York: Academic)
Peart B and Dolder K T 1973 *J. Phys. B: At. Mol. Phys.* **6** 2409
von Busch F and Dunn G H 1972 *Phys. Rev.* A **5** 1726